



OPEN

The high-pressure lithium–palladium and lithium–palladium–hydrogen systems

Mungo Frost^{1✉}, Emma E. McBride^{1,2}, Jesse S. Smith³ & Siegfried H. Glenzer¹

The lithium–palladium and lithium–palladium–hydrogen systems are investigated at high pressures at and above room temperature. Two novel lithium–palladium compounds are found below 18.7 GPa. An ambient temperature phase is tentatively assigned as $F\bar{4}3m$ $\text{Li}_{17}\text{Pd}_4$, with $a = 17.661(1)$ Å at 8.64 GPa, isostructural with $\text{Li}_{17}\text{Sn}_4$. The other phase occurs at high-temperature and is $I\bar{4}3m$ $\text{Li}_{11}\text{Pd}_2$, $a = 9.218(1)$ Å at 3.88 GPa and 200 °C, similar to $\text{Li}_{11}\text{Pt}_2$, which is also known at high pressure. The presence of hydrogen in the system results in an $I\bar{4}3m$ structure with $a = 8.856(1)$ Å at 9.74 GPa. This persists up to 13.3 GPa, the highest pressure studied. Below 2 GPa an fcc phase with a large unit cell, $a = 19.324(1)$ Å at 0.39 GPa, is also observed in the presence of hydrogen. On heating the hydrogen containing system at 4 GPa the $I\bar{4}3m$ phases persists to the melting point of lithium. In both systems melting the lithium results in the loss of crystalline diffraction from palladium containing phases. This is attributed to dissolution of the palladium in the molten lithium, and on cooling the palladium remains dispersed.

Lithium and hydrogen are low Z elements which exhibit complex behaviors at high density, in part due to quantum mechanical effects arising from their low masses^{1,2}. Both have maxima in their melting curves^{3–5} and exhibit complex low symmetry crystal structures, despite their apparent simplicity at low pressure^{6,7}. High pressure metal hydrides have attracted considerable attention recently as various novel compounds have been found to form only at high-pressure^{8,9}, some of which have record breaking high Tc superconductivity^{10,11}.

The alkali metals have also been found to form novel intermetallics at high pressure^{12–16}, with a number of high pressure lithides recently reported^{14–16}. Alkali metals are more electropositive than many other metals, particularly the noble metals, and charge transfer from the alkali metal to the other component of the intermetallic plays a role in their stability^{14,17}.

Various transition metal – lithium intermetallics are reported in the literature at ambient pressure. Typically, these are synthesized by heating the reactants considerably above the melting point of lithium (180 °C at ambient pressure), under an inert atmosphere with characterization performed on quenched products. These have attracted attention due to their potential application in energy storage materials as anode materials for lithium ion batteries¹⁸. Compared to current intercalation type compounds they offer potentially much higher lithium content and hence energy storage potential^{15,18}, motivating the exploration of lithium-rich intermetallic compounds.

Palladium is a transition metal widely used in catalysis and hydrogen purification. The hydrogen affinity of palladium is very sensitive to pressure with palladium hydride, PdH_x , forming below 1 bar. The hydrogen content increases from $x = 0.6$ at formation to $x = 1$ at a few GPa¹⁹. Further compression has not been observed to result in any higher hydride to 100 GPa²⁰. A number of lithium palladium intermetallics have been reported at ambient pressure with stoichiometries of LiPd_7 , LiPd_2 , LiPd , Li_2Pd , Li_3Pd , and $\text{Li}_{15}\text{Pd}_4$ ²¹. All of these were formed at high temperature and quenched to ambient.

Palladium lithium hydride, PdLiH_x , $0.7 < x < 1$, is also known and has been calculated to exhibit superconductivity with the low mass lithium making a large contribution to the electron-phonon coupling²². Subsequent studies have synthesized it but not observed superconductivity. Various synthesis conditions have been used including sintering equimolar mixtures of LiH and Pd in a hydrogen atmosphere at 10 bar²³, heating LiPd in

¹High Energy Density Science Division, SLAC National Accelerator Laboratory, 2575 Sand Hill Road, Menlo Park, USA. ²Stanford PULSE Institute, SLAC National Accelerator Laboratory, 2575 Sand Hill Road, Menlo Park, USA. ³High Pressure Collaborative Access Team, X-ray Science Division, Argonne National Laboratory, Argonne, USA. ✉email: mdffrost@slac.stanford.edu

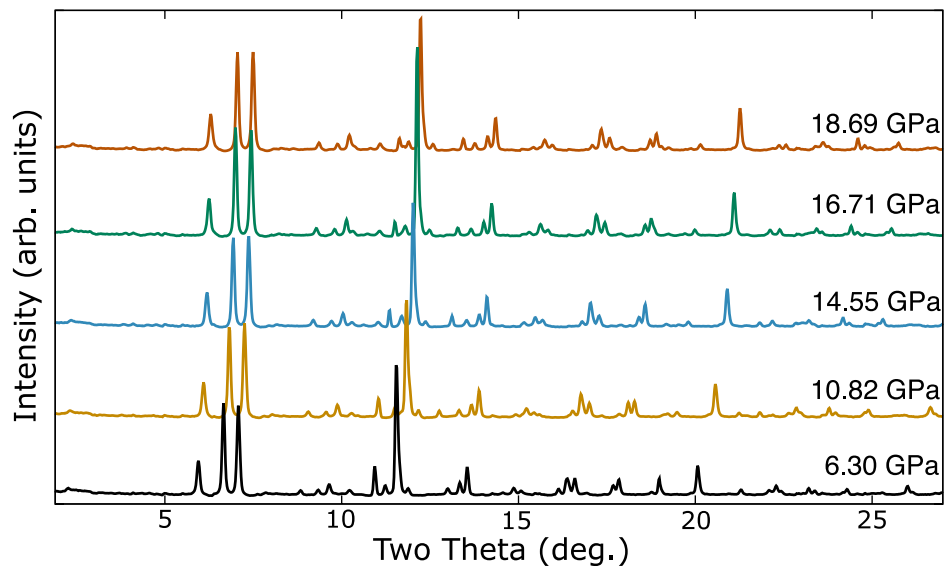


Figure 1. Pressure evolution of the background subtracted integrated diffraction pattern of the lithium–palladium intermetallic at ambient temperature.

270 MPa of hydrogen gas²⁴, and compressing a sealed mixture of LiH and Pd to 3 GPa and heating to 773 K²⁵. These all yield $P4/mmm$ LiPdH_x with x close to 1. Cooling to 4 K at ambient pressure²³, or at 270 MPa²⁴ did not result in superconductivity. Liu et al.²⁵ measured resistivity as a function of temperature and pressure from 2 to 300 K up to 25.2 GPa and observe a minimum in the resistivity with pressure at 18.3 GPa but no superconductivity. They speculate that the discrepancy between theory and experiment may arise from scattering by impurities or hydrogen vacancies.

The application of pressure allows the exploration of exotic chemistry and materials synthesis which does not occur under ambient conditions. To date no study has considered the effect of pressure on the lithium–palladium system, or the lithium–rich lithium–palladium–hydrogen system, nor reported ambient temperature reaction of Pd and Li. Platinum, which lies directly below palladium in the periodic table and shares many properties with it, has been studied under pressure with lithium. It was found to form a $\text{Li}_{11}\text{Pt}_2$ compound with space group $I43m$ below 11 GPa, above which it expels lithium to form $P6/mmm$ Li_2Pt ¹⁴.

Here we study the lithium–rich palladium–lithium and palladium–lithium–hydrogen systems at high pressure, at and above room temperature. All samples exhibited reactions in the cells as loaded, prior to further compression. The initial pressures varied from 0.4 to 6 GPa. We observe two novel compounds which are isostructural with lithium compounds known in other systems. The presence of hydrogen changes the structure adopted by the compound showing it to play a role in the properties of the system. This also demonstrates that the hydrogen affinity of the compound formed is higher than that of pure lithium, which was present in excess in all samples.

Results

Lithium–palladium. In the absence of hydrogen the lithium and palladium had already reacted at after a few days at 5.0 GPa, the lowest pressure measured. Figure 1 shows the pressure evolution of the integrated diffraction patterns collected with 0.4246 Å radiation. These indicate no phase transitions below 18.7 GPa at ambient temperature. The observed peaks cannot be fitted to any known palladium–lithium or platinum–lithium intermetallic. A weak peak at $2\theta = 2.26^\circ$, corresponding to $d = 10.77$ Å, at 6.30 GPa indicates a large unit cell.

Figure 2 shows a LeBail fit²⁶ to an $F43m$ structure with $a = 17.661(1)$ Å at 8.64 GPa. This is similar to known Li_{17}M_4 structures with $\text{M} = \text{Ge}, \text{Sn}, \text{Pb}$, which have $F43m$ symmetry and ambient pressure lattice parameters of 18.756, 19.690, and 19.842 Å respectively²⁷. Close inspection of the LeBail fit reveals a few peaks which are not well fitted, particularly in the region of 8.5 to 10.5 degrees. The lithium–palladium system is known to form numerous intermetallics at ambient pressure and some of these peaks may be due to other low-concentration phases. We do note that a slight tetragonal distortion of the unit cell with $a = 17.656$ Å and $c = 17.869$ Å results in a much improved fit, see Fig. 3, but the symmetry lowering also results in many allowed reflections so this could be pathological. A similarly improved fit, but with even more possible peaks, may be obtained by a monoclinic distortion. The $F43m$ Li_{17}M_4 type structure is the best fit we can obtain to the high-pressure lithium palladium compound, and we tentatively suggest that the structure is this, or closely related to it.

The Li_{17}M_4 structure has $Z = 20$ for a total of 420 atoms per unit cell. This extremely complex structure was previously determined via single crystal X-ray diffraction²⁷. Powder X-ray diffraction in DACs suffers from limited angular range imposed by the geometry of the cell, and limited resolution causing higher angle peaks to overlap. Along with the potential for contaminant peaks this makes a full Rietveld refinement impractical, however a powder X-ray diffraction pattern of the proposed structure can be simulated. Figure 4 compares the observed data with a simulated pattern produced using the literature atomic parameters for $\text{Li}_{17}\text{Sn}_4$ ²⁷, but with

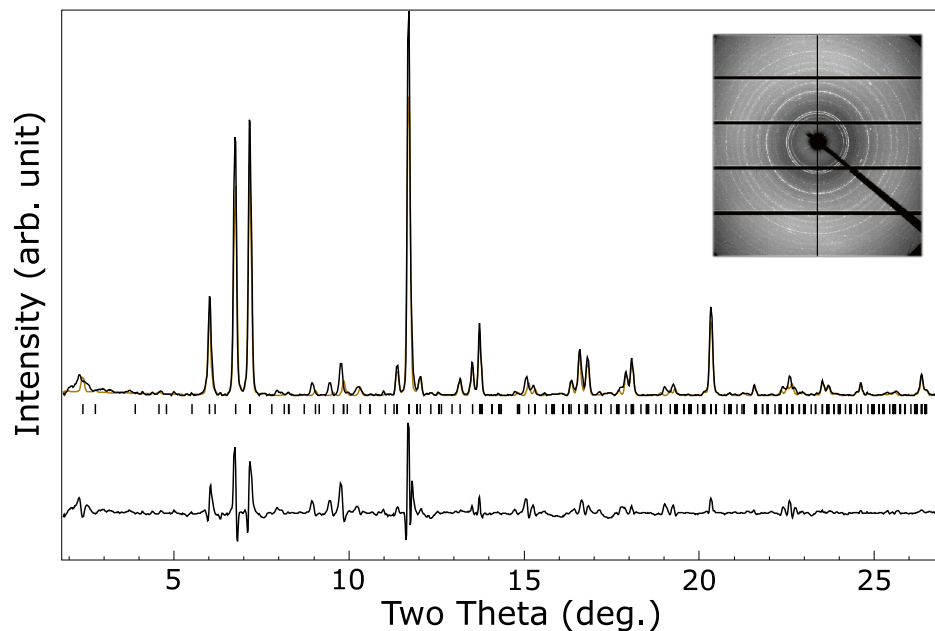


Figure 2. Integrated diffraction pattern of the lithium–palladium intermetallic at ambient temperature and 8.64 GPa (black), with LeBail fit to $F\bar{4}3m$ phase with $a = 17.661 \text{ \AA}$ (orange) and residual on same scale (lower black line). Allowed peak positions are indicated by ticks. See text for discussion of fit. *Inset:* Unintegrated diffraction pattern.

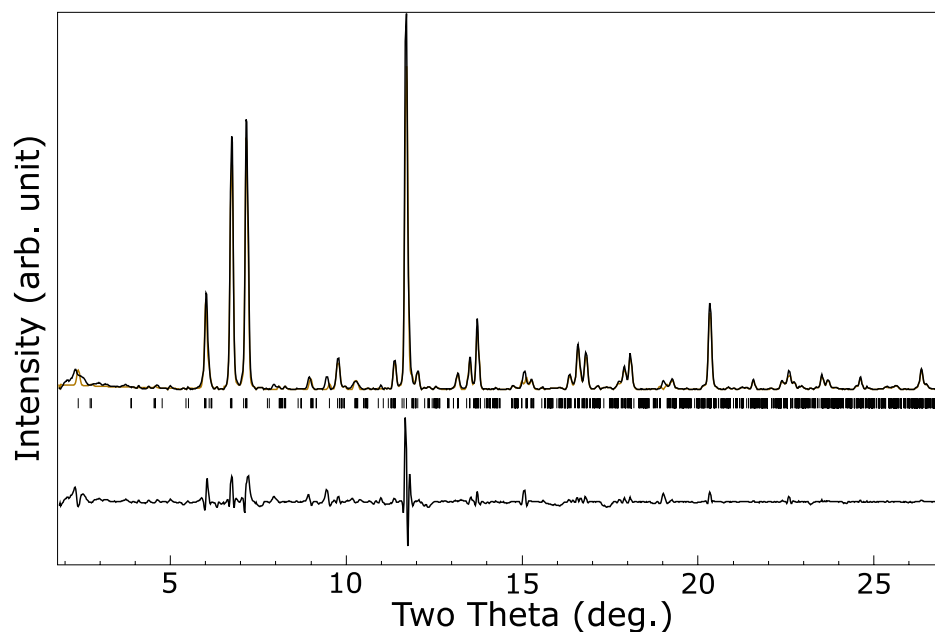


Figure 3. Integrated diffraction pattern of the lithium–palladium intermetallic at ambient temperature and 8.64 GPa (black), with LeBail fit to a face centered tetragonal phase with $a = 17.656$ and $c = 17.868 \text{ \AA}$ (orange) and residual on same scale (lower black line). Allowed peak positions are indicated by ticks. The unit cell is expressed as face centered tetragonal rather than the equivalent, smaller volume, body centered tetragonal cell to aid comparison to the $F\bar{4}3m$ phase fitted in Fig. 2.

Sn exchanged for Pd and the lattice parameter set to match that LeBail fitted to the observed data. The patterns are quite similar which supports the $F\bar{4}3m \text{ Li}_{17}\text{Pd}_4$ structural candidate for the novel palladium lithide.

On heating at 4 GPa the appearance of the pattern changes with new peaks appearing at 200 °C, see Fig. 5. This pattern can be fitted as a mixture of the ambient temperature $F\bar{4}3m$ phase and a bcc phase with $a = 9.218(1) \text{ \AA}$ at 3.88 GPa. This is compatible with $I\bar{4}3m$ symmetry and consideration of the density suggests it is $\text{Li}_{11}\text{Pd}_2$,

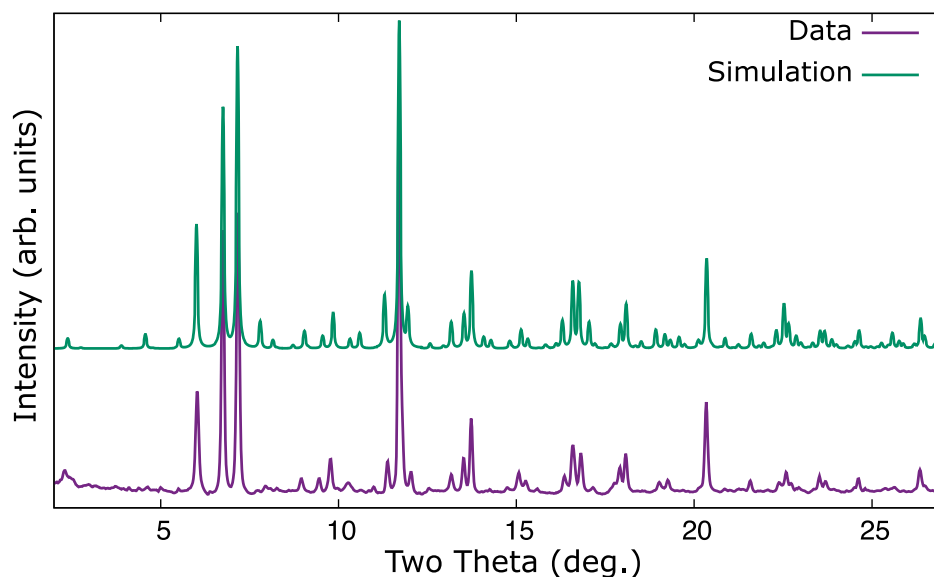


Figure 4. Comparison of observed data from a lithium–palladium mixture at 8.64 GPa (lower trace) and a simulated powder pattern (upper trace) of $F\bar{4}3m$ $\text{Li}_{17}\text{Pd}_4$ using the atomic parameters from $\text{Li}_{17}\text{Sn}_4$ ²⁷ and lattice parameter and radiation from this study. The similarity supports the novel palladium–lithium compound having a similar structure to $\text{Li}_{17}\text{Sn}_4$.

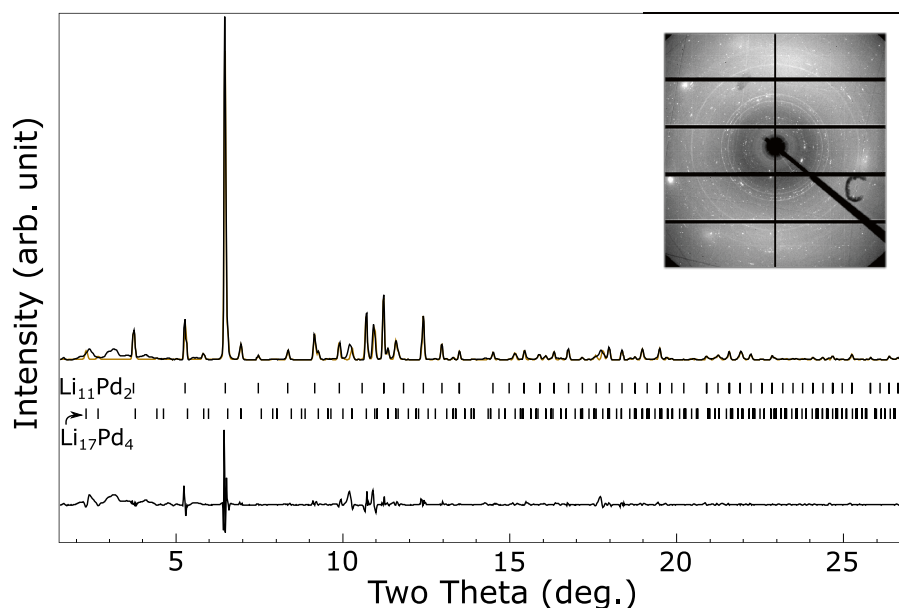


Figure 5. Integrated diffraction pattern of the lithium–palladium intermetallics at 200 °C and 3.88 GPa (black), with LeBail fit to proposed ambient-temperature $F\bar{4}3m$ $\text{Li}_{17}\text{Pd}_4$ ($a = 18.229$ Å) and high-temperature $I\bar{4}3m$ $\text{Li}_{11}\text{Pd}_2$ ($a = 9.218$ Å) phases (orange) and residual on same scale (lower black line). Allowed peak positions for each phase are indicated by ticks. The broad unfitted features at low angle are from the Kapton window of the heater. *Inset:* Unintegrated diffraction pattern.

isostructural with $\text{Li}_{11}\text{Pt}_2$ observed in the high pressure lithium–platinum system¹⁴. This phase has a γ -brass structure and has been observed in other palladium-group intermetallics^{28,29}.

Further heating to 225 °C melts the lithium and leads to the loss of all crystalline diffraction from palladium. We attribute this to dissolution of the palladium into the large excess of lithium. On cooling, peaks from bcc -lithium reappear, however, those from the palladium intermetallic do not, nor do any new peaks appear. The most likely explanation for the loss of diffraction from the palladium is that it is incorporated into the large excess of bcc lithium. Further compression causes the bcc to fcc transition in lithium near 7.5 GPa, as expected³⁰, but no peaks other than those of fcc -lithium emerge implying that the palladium remains dispersed.

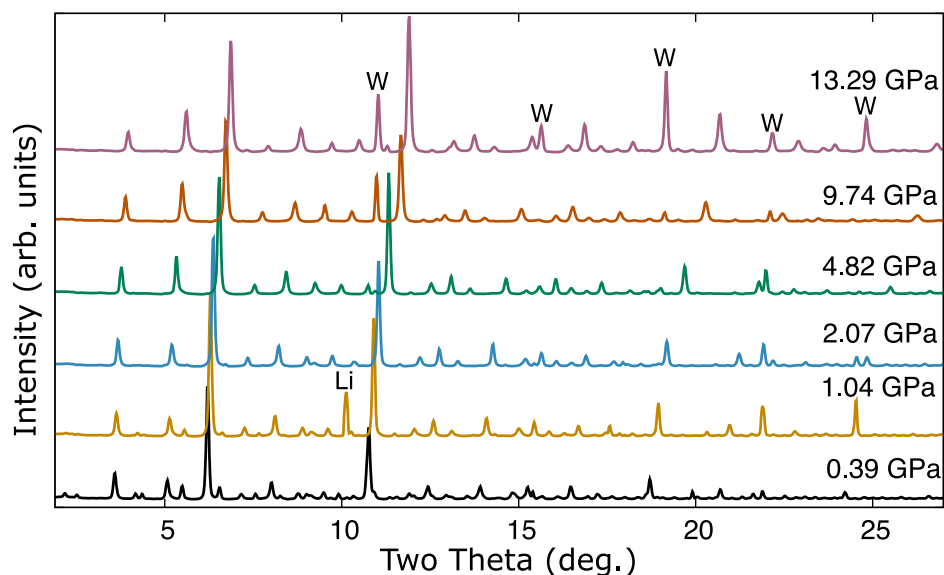


Figure 6. Pressure evolution of the background subtracted integrated diffraction patterns of the lithium–palladium–hydrogen system at ambient temperature. The peaks marked W in the highest trace are due to tungsten and are present at similar angles in some lower pressure traces. A strong lithium peak is also marked at 1.04 GPa.

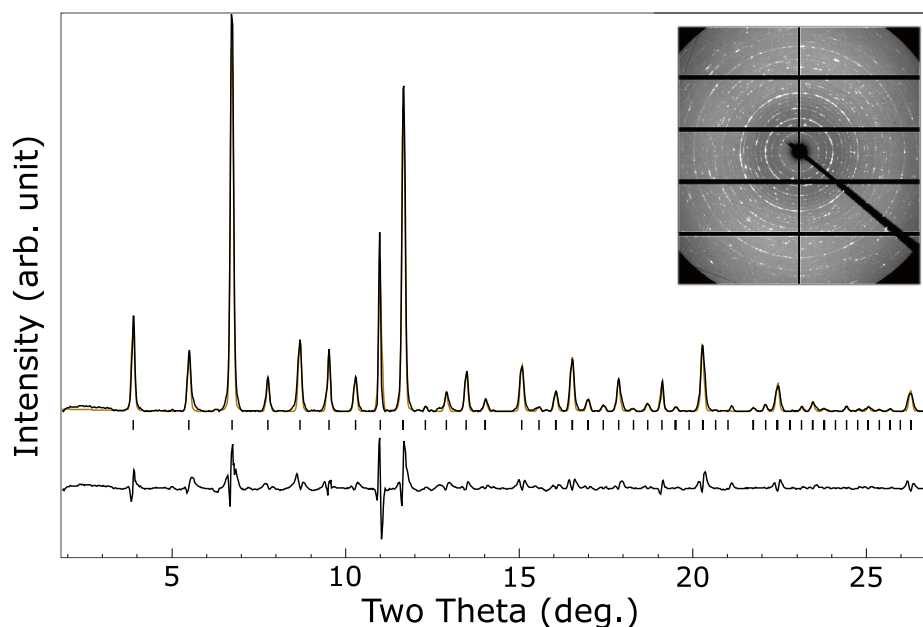


Figure 7. Integrated diffraction pattern of the lithium–palladium–hydrogen intermetallic at ambient temperature and 9.74 GPa (black), with LeBail fit to $I43m$ phase ($a = 8.856 \text{ \AA}$) (orange) and residual on same scale (lower black line). Allowed peak positions are indicated by ticks. *Inset:* Unintegrated diffraction pattern.

Lithium–palladium–hydrogen. The presence of hydrogen in cells loaded with palladium, lithium and lithium hydride stabilized different phases under pressure, with a transition occurring between 1 and 2 GPa, see Fig. 6. Above the transition a single phase is observed. This is well fitted by a bcc structure with and $a = 8.856(1) \text{ \AA}$ at 9.74 GPa, compatible with $I43m$ symmetry, similar to the $\text{Li}_{11}\text{Pd}_2$ phase observed at high-temperature in the lithium–palladium system. An integrated pattern and LeBail fit are shown in Fig. 7. Below 2 GPa a second set of peaks are observed, see Fig. 6, which are fitted by an fcc phase with a large unit cell of $a = 19.324(1) \text{ \AA}$ at 0.39 GPa. A LeBail fit is shown in Fig. 8. The stoichiometry of the compounds cannot be determined, though hydrogen must be present to cause the structural differences from the lithium–palladium system. Figure 9 shows the similarity between observed diffraction pattern of the bcc phase and simulated powder data based on the structure of $I43m \text{ Li}_{11}\text{Pt}_2$ ¹⁴.

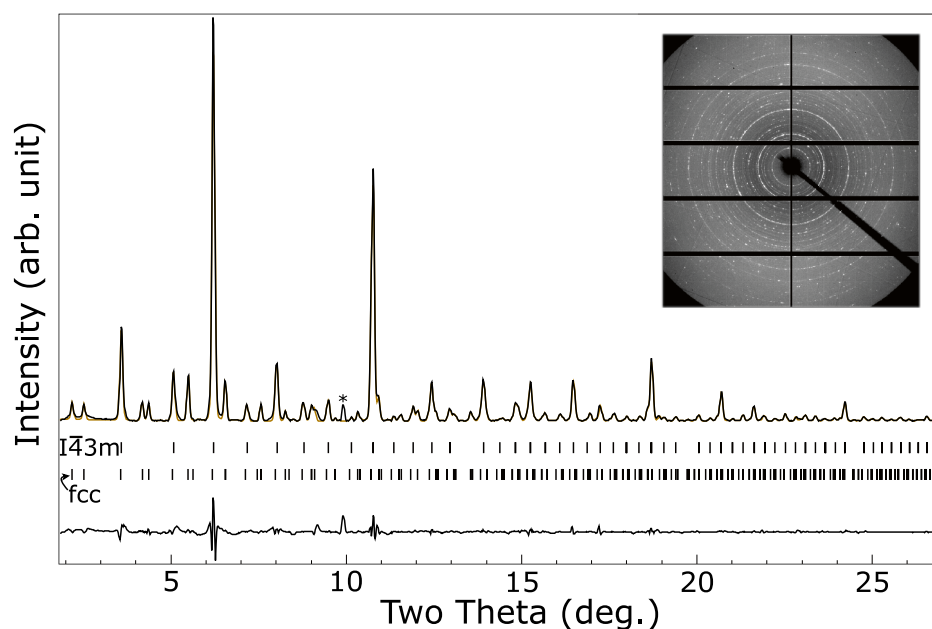


Figure 8. Integrated diffraction pattern of the lithium–palladium–hydrogen intermetallics at ambient temperature and 0.39 GPa (black), with LeBail fit to the low-pressure *fcc* phase ($a = 19.324 \text{ \AA}$) and the high-pressure *I43m* phase ($a = 9.597 \text{ \AA}$) and residual on same scale (lower black line). Allowed peak positions for each phase are indicated by ticks. The unfitted peak marked with an asterisk is the (110) reflection from *bcc*-lithium. *Inset:* Unintegrated diffraction pattern.

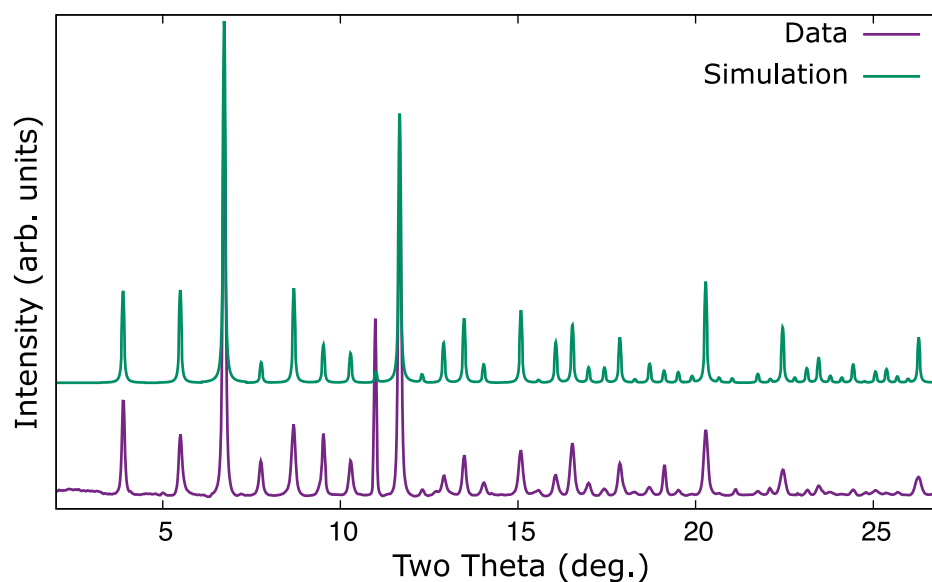


Figure 9. Comparison of observed data from a lithium–palladium–hydrogen mixture at 9.74 GPa (lower trace) and a simulated powder pattern (upper trace) of *I43m* $\text{Li}_{11}\text{Pd}_2$ using the atomic parameters from $\text{Li}_{11}\text{Pt}_2$ ¹⁴ and lattice parameter and radiation from this study. The similarity supports the palladium–lithium–hydrogen compound having a similar structure to $\text{Li}_{11}\text{Pt}_2$.

Between 0.4 GPa, the lowest pressure the palladium, lithium and lithium hydride system was studied at, and 1 GPa an additional *fcc* phase with a large unit cell is present, see fit in Fig. 8. This is similar to the *F43m* $\text{Li}_{17}\text{Pd}_4$ phase proposed for the lithium–palladium system, and may be a related structure. The peaks from this phase are weak by 1 GPa and absent at 2 GPa.

On heating at 4 GPa, the hydride containing sample showed no phase changes below the melting point of lithium. On melting the lithium, the palladium dissolves, as for the lithium–palladium system, and remains dispersed on cooling.

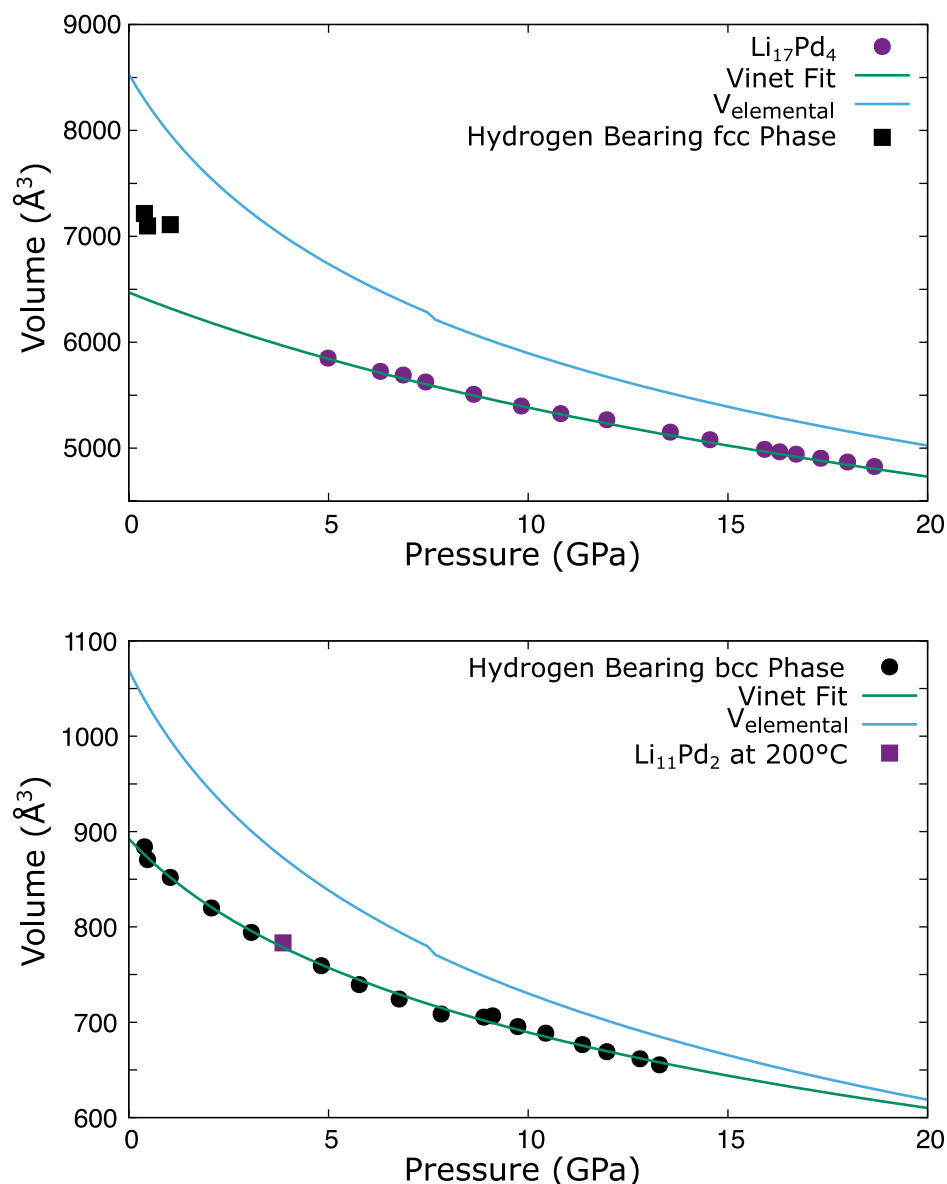


Figure 10. Volume vs pressure plots. Top: the $\text{Li}_{17}\text{Pd}_4$ $F\bar{4}3m$ phase (fuchsia circles) and low-pressure fcc hydrogen bearing phase (black squares). The green line is a Vinet fit to the circle points, note that hydrogen bearing fcc phase lies off this curve. The blue line is the volume of an equivalent number of lithium (340) and palladium (80) atoms in the elemental form^{20,30,32}. Bottom: the bcc hydrogen bearing phase (black circles) and $\text{Li}_{11}\text{Pd}_2$ $I43m$ phase at 200 °C (fuchsia square). The green Vinet fit is to the circle points. The blue line is the volume of 44 lithium and 8 palladium atoms in elemental form, corresponding to $\text{Li}_{11}\text{Pd}_2$. The discontinuity near 8 GPa lies close to the bcc to fcc transition in lithium and may indicate a change in stoichiometry.

Discussion

Without hydrogen the lithium–palladium system forms an ambient temperature structure we tentatively assign to be of $F43m$ symmetry and isostructural with $\text{Li}_{17}\text{Sn}_4$. Interpretation of the powder pattern, Fig. 2, is hindered by the possibility of additional phases or small distortions of the unit cell. Comparison to a simulated pattern for $\text{Li}_{17}\text{Pd}_4$, Fig. 4, suggests the observed structure is the same, or closely related. This structure has not been observed in any other transition metal - alkali metal intermetallic, however it is observed in the lithides of silicon, germanium, tin and lead^{27,31} with slightly varying stoichiometry.

Volumetric considerations give further support for the structures of both $\text{Li}_{17}\text{Pd}_4$ and $\text{Li}_{11}\text{Pd}_2$ assigned from comparison of the diffraction data to other known lithides. Figure 10 shows pressure-volume data collected on compression for both phases, complete with fitted equations of state of the Vinet form:

Phase	$V_0(\text{\AA}^3)$	B_0 (GPa)	B'_0
$F\bar{4}3m$ Li ₁₇ Pd ₄	6471(48)	43.9(39)	2.63(42)
bcc hydrogen bearing phase	892.6(92)	19.6(29)	5.45(72)

Table 1. Fitted Vinet equation of state parameters.

Compound	$V/V_{\text{elemental}}$	Conditions	Ref.
$F\bar{4}3m$ Li ₁₇ Pd ₄	0.76	0 GPa	This study
$F\bar{4}3m$ Li ₁₇ Pd ₄	0.87	5 GPa	This study
$F\bar{4}3m$ Li ₁₇ Pd ₄	0.91	10 GPa	This study
$I\bar{4}3m$ Li ₁₁ Pd ₂	0.90	3.86 GPa, 200 °C	This study
$I\bar{4}3d$ Li ₁₅ Pd ₄	0.71	Ambient	²¹
$Fm\bar{3}m$ Li ₃ Pd	0.74	Ambient	²¹
$P6/mmm$ Li ₂ Pd	0.73	Ambient	²¹
$Pm\bar{3}m$ LiPd	0.73	Ambient	²¹
$P\bar{6}$ LiPd	0.75	Ambient	²¹
$Fm\bar{3}m$ LiPd ₇	0.90	Ambient	²¹

Table 2. Comparison of the ratio of the volume of various lithium–palladium intermetallics to the volume of an equivalent quantity of elemental lithium and palladium. Temperature is ambient except where noted. Volumes for Li₁₇Pd₄ from this study are based on its equation of state.

$$P = 3B_0 \left(\frac{1 - \left(\frac{V}{V_0}\right)^{\frac{1}{3}}}{\left(\frac{V}{V_0}\right)^{\frac{2}{3}}} \right) e^{\frac{3}{2}(B'_0 - 1) \left(1 - \left(\frac{V}{V_0}\right)^{\frac{1}{3}}\right)}$$

Where B_0 and V_0 are the zero-pressure bulk modulus and volume, V is the volume at pressure P , and B'_0 is the pressure derivative of the bulk modulus. The fitted equation of state parameters are given in Table 1. Both compounds exhibit intermediate compressibility between those of lithium, which is highly compressible^{30,32}, and palladium, which has low compressibility²⁰.

Figure 10 also shows the pressure-volume curves for the pure elements at the proposed stoichiometries. In both cases the compounds are denser, with the difference decreasing at higher pressure. Table 2 gives the ratio of the volume of palladium–lithium intermetallics to their elemental constituents and shows the increased density of the intermetallics in this study to be within the range of expected values. In the solid phase the pressure-volume curve of a compound is expected to lie close to that of its constituents of enthalpic grounds. Excess volume will have an increasingly punitive PV term in its free energy, while overly reduced volume would lead to unphysical densities.

In the presence of hydrogen two phases are observed. At low pressure an fcc phase with a large unit cell ($a = 19.324 \text{ \AA}$ at 0.39 GPa) coexists with a phase which appears similar to the $I\bar{4}3m$ Li₁₁M₂ phase observed in the lithium–platinum system¹⁴ and lithium–palladium at high-pressure and high-temperature. Above 1 GPa the fcc phase is lost and only the $I\bar{4}3m$ phase remains. The volume of the low pressure fcc phase observed in the hydride containing system lies off the curve of the Li₁₇Pd₄ produced without hydrogen present and both cannot be fitted to a single equation of state. This could arise from hydrogen absorbed into the lattice, or may indicate they have different structures.

Both lithium and hydrogen are low Z and so scatter X-rays very weakly compared to palladium. Therefore, we would not expect to be able to resolve partial replacement of lithium by hydrogen, or additional hydrogen incorporated into the lattice, except on volumetric grounds. This makes the stoichiometries of the phases formed in the palladium–lithium–hydrogen samples impossible to determine, and non-stoichiometric phases cannot be ruled out. Examination of the patterns and comparison to the high temperature lithium–palladium system, and to the literature on the lithium–platinum system, strongly supports the structure being an analog to the $I\bar{4}3m$ Li₁₁M₂ ($M = \text{Pt, Pd}$) γ -brass structure. The high-temperature $I\bar{4}3m$ Li₁₁Pd₂ phase which forms in the absence of hydrogen has similar volume to the hydrogen bearing $I\bar{4}3m$ phase, see Fig. 10. This limits the quantity of additional hydrogen which can be present and suggests that the structural differences are caused either by substitution of lithium with hydrogen, or very dilute hydrogen present in the lattice. The inclusion of trace impurities has previously been suggested to change the structure of LiPd at ambient pressure²¹. Inspection of the pressure-volume data of the hydrogen containing $I\bar{4}3m$ structure shows a slight discontinuity at 8 GPa, this is likely due to small compositional changes such as the incorporation of additional hydrogen, as the diffraction patterns above and below this appear similar.

A $\text{Li}_{15}\text{Pd}_4$ palladium–lithium intermetallic with $I\bar{4}3d$ symmetry has been reported at ambient pressure²¹ with $a = 10.676 \text{ \AA}$. This is not compatible with any diffraction patterns observed in this study. The high-temperature $\text{Li}_{11}\text{Pd}_2$ and related hydrogen containing $I43m$ phase both have several peaks which are incompatible with the $I\bar{4}3d$ space group. Van Vucht and Buschow²¹ observed an unknown F-centered cubic lithium–palladium intermetallic with $a = 19.009 \text{ \AA}$ at 10 to 16 at% Pd. While they did not observe satisfactory agreement with the $\text{Li}_{17}\text{Pb}_4$ structure (wrongly assigned as the $\text{Li}_{22}\text{Pb}_5$ structure at the time of their publication²⁷) it is possible their *fcc* phase is the same as, or related to, the one we observe here at higher pressure.

The study of transition metal hydrides and lithides is of interest to various fields including hydrogen storage³³, battery technology^{18,34} and superconductivity²². The phases reported here present a test for theory at high pressure, particularly given the large body of work which exists on the binary hydrides of lithium and palladium^{19,20,33,35}. The reactivity of lithium, lithium hydride and palladium is also relevant to hydrogen storage as both lithium and palladium have proposed applications in the hydrogen economy^{33,36}.

In conclusion, we investigated the palladium–lithium and palladium–lithium–hydrogen systems to 18.7 and 13.3 GPa respectively. The palladium–lithium system reveals a single intermetallic at ambient temperature which we tentatively assign to an $F43m$ Li_{17}M_4 type structure, possibly with a small distortion. At 200 °C at 3.87 GPa this partially converts to an $I43m$ $\text{Li}_{11}\text{Pd}_2$ structure analogous to $\text{Li}_{11}\text{Pt}_2$ in the dense lithium–platinum system. The palladium–lithium–hydrogen system forms an $I\bar{4}3m$ structure similar to $\text{Li}_{11}\text{Pd}_2$ at all pressures and temperatures studied. Below 2 GPa we also observe an *fcc* phase with a large unit cell in this system. Due to the weak scattering from hydrogen and lithium it is not possible to determine the stoichiometries, though volumetric considerations disallow high concentrations of additional hydrogen in the $I\bar{4}3m$ phase. On heating to the melting point of lithium, diffraction from the palladium compounds disappears in both systems and does not reappear on cooling. This is attributed to the palladium forming a dilute solid solution in the large excess of lithium metal.

Methods

Diamond anvil cells (DACs) were prepared with rhenium gaskets on Boehler-Almax type diamond anvils with culet sizes ranging from 250 to 400 μm . Pressure was determined to an uncertainty of 0.1 GPa via the temperature adjusted equation of state³⁷ of a small quantity of tungsten powder (Alfa Aesar, 99.9%) added to each loading. Tungsten was chosen as it is known not to react with lithium^{4,30}, and does not form hydrides below 25 GPa⁹. Powdered palladium (Alfa Aesar, 99.95%) was added to each cell such that the lithium would be in large excess. Lithium metal (Alfa Aesar, 99.9%) and, for hydrogen containing cells lithium hydride (Alfa Aesar, 99.4%), were loaded under a high purity argon atmosphere. Hydrogen was introduced as lithium hydride because lithium metal fully reacts with hydrogen gas at pressures below 50 MPa³⁵ making gas loading an unnecessary complication. The maximum pressure was 18.7 GPa to avoid damage to the diamond anvils by lithium at higher pressure^{3,30,32}. There was no evidence of reactions involving the tungsten pressure marker, diamond anvils or rhenium gasket in any cell, nor was there any observable reaction between the lithium and lithium hydride.

Angular dispersive powder X-ray diffraction measurements were carried out at APS beamline 16-ID-B (HPCAT) using 0.4246 \AA radiation. Full diffraction maps were taken by rastering the samples with 5 μm steps taking a diffraction pattern at each location to ensure purity of the loadings. The load on the cells was controlled using a gas membrane with patterns collected on a Dectris Pilatus 1M large area detector with a sample to detector distance of 200 mm and 172 μm pixels. Resistive heating was performed under vacuum with Kapton X-ray windows using the HPCAT resistive heating setup³⁸. Temperature was determined with uncertainty of $\pm 3 \text{ }^\circ\text{C}$ using two type K thermocouples in contact with the cell. Ambient temperature runs were performed in air without the Kapton windows.

Diffraction patterns were integrated using the DIOPRAS software package³⁹. The integrated patterns were further analyzed using JANA06⁴⁰ and POWDERCELL⁴¹. LeBail fits determine the unit cell parameters based on the angles of the powder diffraction peaks and can give information on the space group based on systematic absences²⁶, but do not offer details on the location of atoms within the cell. LeBail fits were performed as the complex structures of the intermetallics formed, and limited q-range and resolution possible in diamond anvil cells, made Rietveld fits unstable. Strain and preferred orientation also cannot be ruled out, particularly as the compounds were formed in situ under pressure.

Data availability

The datasets used and/or analysed during the current study available from the corresponding author on reasonable request.

Received: 29 April 2022; Accepted: 13 July 2022

Published online: 19 July 2022

References

1. Neaton, J. & Ashcroft, N. Pairing in dense lithium. *Nature* **400**, 141–144 (1999).
2. Bonev, S. A., Schwegler, E., Ogitsu, T. & Galli, G. A quantum fluid of metallic hydrogen suggested by first-principles calculations. *Nature* **431**, 669–672 (2004).
3. Schaeffer, A. M. J., Talmadge, W. B., Temple, S. R. & Deemyad, S. High pressure melting of lithium. *Phys. Rev. Lett.* **109**, 185702 (2012).
4. Frost, M. *et al.* High-pressure melt curve and phase diagram of lithium. *Phys. Rev. Lett.* **123**, 065701 (2019).
5. Howie, R. T., Dalladay-Simpson, P. & Gregoryanz, E. Raman spectroscopy of hot hydrogen above 200 GPa. *Nat. Mater.* **14**, 495–499 (2015).
6. Guillaume, C. L. *et al.* Cold melting and solid structures of dense lithium. *Nat. Phys.* **7**, 211–214 (2011).
7. Loubeyre, P., Occelli, F. & Dumas, P. Synchrotron infrared spectroscopic evidence of the probable transition to metal hydrogen. *Nature* **577**, 631–635 (2020).

8. Matsuoka, T. *et al.* Beryllium polyhydride $\text{Be}_4\text{H}_8(\text{H}_2)_2$ synthesized at high pressure and temperature. *Phys. Rev. Mater.* **4**, 125402 (2020).
9. Scheler, T. *et al.* Nanocrystalline tungsten hydrides at high pressures. *Phys. Rev. B* **87**, 184117 (2013).
10. Drozdov, A. *et al.* Superconductivity at 250 K in lanthanum hydride under high pressures. *Nature* **569**, 528–531 (2019).
11. Drozdov, A., Erements, M., Troyan, I., Ksenofontov, V. & Shylin, S. I. Conventional superconductivity at 203 Kelvin at high pressures in the sulfur hydride system. *Nature* **525**, 73–76 (2015).
12. Du, X., Lou, H., Wang, J. & Yang, G. Pressure-induced Na–Au compounds with novel structural units and unique charge transfer. *Phys. Chem. Chem. Phys.* **23**, 6455–6461 (2021).
13. Frost, M., McBride, E. E., Schörner, M., Redmer, R. & Glenzer, S. H. Sodium–potassium system at high pressure. *Phys. Rev. B* **101**, 224108 (2020).
14. Binns, J. *et al.* Reactivity of lithium and platinum at elevated densities. *Phys. Rev. B* **99**, 220101 (2019).
15. Dalladay-Simpson, P. *et al.* Structures of lithium–zinc compounds at high pressures. *J. Chem. Phys.* **149**, 024306 (2018).
16. Botana, J. & Miao, M.-S. Pressure-stabilized lithium caesides with caesium anions beyond the -1 state. *Nat. Commun.* **5**, 1–8 (2014).
17. Spicer, W., Sommer, A. & White, J. Studies of the semiconducting properties of the compound CSAU. *Phys. Rev.* **115**, 57 (1959).
18. Obrovac, M. & Chevri er, V. Alloy negative electrodes for Li-ion batteries. *Chem. Rev.* **114**, 11444–11502 (2014).
19. Manchester, F., San-Martin, A. & Pitre, J. The H–Pd (hydrogen–palladium) system. *J. Phase Equilib.* **15**, 62–83 (1994).
20. Guigue, B., Geneste, G., Leridon, B. & Loubeyre, P. An X-ray study of palladium hydrides up to 100 GPa: Synthesis and isotopic effects. *J. Appl. Phys.* **127**, 075901 (2020).
21. Van Vucht, J. & Buschow, K. Note on the occurrence of intermetallic compounds in the lithium–palladium system. *J. Less Common Metals* **48**, 345–347 (1976).
22. Singh, D., Cohen, R. & Papaconstantopoulos, D. Possibility of LiPdH_x as a new ionic superconductor. *Phys. Rev. B* **41**, 861 (1990).
23. Nor eus, D. & Rapp,  . Absence of superconductivity above 4 K in LiPdH_x . *Phys. Rev. B* **42**, 10730 (1990).
24. Schirber, J., Overmyer, D., Baughman, R. & Morosin, B. Search for high temperature superconductivity in LiPdH_x . *Phys. C Supercond.* **172**, 465–466 (1991).
25. Liu, W. *et al.* Absence of superconductivity in LiPdH_x . *Philos. Mag.* **98**, 623–631 (2018).
26. Le Bail, A. Whole powder pattern decomposition methods and applications: A retrospection. *Powder Diffract.* **20**, 316–326 (2005).
27. Goward, G., Taylor, N., Souza, D. & Nazar, L. The true crystal structure of Li_i7M_4 ($\text{M} = \text{Ge, Sn, Pb}$)-revised from Li_22M_5 . *J. Alloys Compd.* **329**, 82–91 (2001).
28. Gourdon, O. & Miller, G. J. Intergrowth compounds in the Zn–rich Zn–Pd system: Toward 1D quasicrystal approximants. *Chem. Mater.* **18**, 1848–1856 (2006).
29. Harbrecht, B., Thimmaiah, S., Armbr uster, M., Pietzonka, C. & Lee, S. Structure and properties of γ -brass-type $\text{Pt}_2\text{Zn}_11-\delta$ ($0.2 < \delta < 0.3$). *Zeitschrift f ur anorganische und allgemeine Chemie* **628**, 2744–2749 (2002).
30. Frost, M., Levitan, A. L., Sun, P. & Glenzer, S. Equation of state and electron localisation in fcc lithium. *J. Appl. Phys.* **123**, 065901 (2018).
31. Zeilinger, M., Benson, D., Haussermann, U. & F assler, T. F. Single crystal growth and thermodynamic stability of Li_i7Si_4 . *Chem. Mater.* **25**, 1960–1967 (2013).
32. Hanfland, M., Loa, I., Syassen, K., Schwarz, U. & Takemura, K. Equation of state of lithium to 21 GPa. *Solid State Commun.* **112**, 123–127 (1999).
33. Banger, S., Nayak, V. & Verma, U. Hydrogen storage in lithium hydride: A theoretical approach. *J. Phys. Chem. Solids* **115**, 6–17 (2018).
34. Sun, K. & Peng, Z. Intermetallic interphases in lithium metal and lithium ion batteries. *InfoMat* **3**, 1083–1109 (2021).
35. Howie, R. T., Narygina, O., Guillaume, C. L., Evans, S. & Gregoryanz, E. High-pressure synthesis of lithium hydride. *Phys. Rev. B* **86**, 064108 (2012).
36. Schneemann, A. *et al.* Nanostructured metal hydrides for hydrogen storage. *Chem. Rev.* **118**, 10775–10839 (2018).
37. Litasov, K. D. *et al.* Thermal equation of state to 33.5 GPa and 1673 K and thermodynamic properties of tungsten. *J. Appl. Phys.* **113**, 133505 (2013).
38. Sinogeikin, S. V. *et al.* Online remote control systems for static and dynamic compression and decompression using diamond anvil cells. *Rev. Sci. Instrum.* **86**, 072209 (2015).
39. Prescher, C. & Prakapenka, V. B. Dioptas: A program for reduction of two-dimensional X-ray diffraction data and data exploration. *High Pressure Res.* **35**, 223–230 (2015).
40. Petri cek, V., Du ek, M. & Palatinus, L. Crystallographic computing system JANA2006: General features. *Zeitschrift f ur Kristallographie-Crystalline Materials* **229**, 345–352 (2014).
41. Kraus, W. & Nolze, G. Powder cell—a program for the representation and manipulation of crystal structures and calculation of the resulting X-ray powder patterns. *J. Appl. Crystallogr.* **29**, 301–303 (1996).

Acknowledgements

The authors would like to thank Eric Rod and Curtis Kenney-Benson. This work was supported by U.S. Department of Energy (DOE) Office of Fusion Energy Sciences funding No. FWP100182. This work was supported by the Department of Energy, Laboratory Directed Research and Development program at SLAC National Accelerator Laboratory, under contract DE-AC02-76SF00515 and as part of the Panofsky Fellowship awarded to E.E.M. Equipment support from Stanford Synchrotron Radiation Light source (SSRL) is acknowledged under DOE Office of Basic Energy Sciences under Contract No. DE-AC02-76SF00515. X-ray diffraction was performed at HPCAT (Sector 16), Advanced Photon Source (APS), Argonne National Laboratory. HPCAT operations are supported by DOE-NNSA’s Office of Experimental Sciences. The Advanced Photon Source is a U.S. Department of Energy (DOE) Office of Science User Facility operated for the DOE Office of Science by Argonne National Laboratory under Contract No. DE-AC02-06CH11357.

Author contributions

M.F. and S.H.G. conceived the experiment, M.F. and E.E.M. conducted the experiments, J.S. tested and modified equipment and M.F. analysed the results and wrote the manuscript. All authors reviewed the manuscript.

Competing interests

The authors declare no competing interests.

Additional information

Correspondence and requests for materials should be addressed to M.F.

Reprints and permissions information is available at www.nature.com/reprints.

Publisher's note Springer Nature remains neutral with regard to jurisdictional claims in published maps and institutional affiliations.



Open Access This article is licensed under a Creative Commons Attribution 4.0 International License, which permits use, sharing, adaptation, distribution and reproduction in any medium or format, as long as you give appropriate credit to the original author(s) and the source, provide a link to the Creative Commons licence, and indicate if changes were made. The images or other third party material in this article are included in the article's Creative Commons licence, unless indicated otherwise in a credit line to the material. If material is not included in the article's Creative Commons licence and your intended use is not permitted by statutory regulation or exceeds the permitted use, you will need to obtain permission directly from the copyright holder. To view a copy of this licence, visit <http://creativecommons.org/licenses/by/4.0/>.

© The Author(s) 2022